Supporting Information:

TaO$_x$ electron transport layers

for CO$_2$ reduction Si photocathodes

Rajiv Ramanujam Prabhakar,[a,b,#] Raphaël Lemerle,[a,b,c,#] Magda Barecka,[d,e,f] Minki Kim,[a,b,g]

Sehun Seo[a,b], Elif Nur Dayi,[a,b,c] Irene Dei Tos,[a,b] and Joel W. Ager,[a,b,h,i,]*

[a]Liquid Sunlight Alliance, Lawrence Berkeley National Laboratory, Berkeley, California 94720, United States

[b]Chemical Sciences Division, Lawrence Berkeley National Laboratory, Berkeley, California 94720, United States

[c]Materials Science and Engineering, École Polytechnique Fédéral de Lausanne, Lausanne 1015, Switzerland

[d]Department of Chemical Engineering, Northeastern University, 360 Huntington Avenue, 02215 Boston, USA; email: m.barecka@northeastern.edu

[e]Department of Chemistry and Chemical Biology, Northeastern University, 360 Huntington Avenue, 02215 Boston, USA

[f]Cambridge Centre for Advanced Research and Education in Singapore, CARES Ltd., 1 CREATE Way, CREATE Tower #05-05, 138602, Singapore.

[g]Chemical and Biomolecular Engineering, Korea Advanced Institute of Science and Technology (KAIST), Daejeon 34141, Republic of Korea

[h]Department of Materials Science and Engineering, University of California, Berkeley, Berkeley, CA 94720, USA

[i]Materials Sciences Division, Lawrence Berkeley National Laboratory, Berkeley, California 94720, United States

# These authors contributed equally

*jwager@lbl.gov (J. W. Ager)

Table of Contents

Silicon substrate preparation

The Silicon wafers were cleaned by sonication in acetone (10 min), soap water (10 min), deionized water (10 min) and iso-propyl alcohol (10 min), in that order. After this, they were etched to remove the native oxide layer by dipping the silicon wafers in 1% HF for 5 min. Particular emphasis was placed to make sure that immediately after the HF treatment, the wafers were either loaded into the PLD chamber or sputtering chamber to prepare the p-Silicon photocathodes. For preparation of p-Si with n^+ (phosphorus) doping - Phosphorus ions with energies of 50 keV and 30 keV and corresponding doses of $2x10^{14}$ and $1x10^{14}$ cm^{-2} were used to form the n^+ layer. The implanted wafers were then annealed at 950 °C for 30 sec in a rapid thermal annealing (RTA) furnace. n-Si photocathodes with n^+ and p^+ implants were fabricated using the procedure described elsewhere.[1]

Atomic layer deposition of TiO_2

TiO_2 was deposited by ALD onto p-Si wafers using a titanium tetraisopropoxide (TTIP) as the Ti precursor and water as the oxygen source with a thickness of 20 nm (measured by ellipsometry) at a temperature of 125°C.

Synthesis of TaO_x by pulsed laser deposition

TaO_x was deposited onto p-Si wafers using a pure Ta_2O_5 target by PLD (KrF laser 248nm) using a procedure reported in literature.[2] The PLD laser frequency was set to 10 Hz and the energy was set at 150 mJ. The oxygen flow rate during deposition was varied from 0.1 to 1.6 sccm. Corresponding oxygen pressure in the PLD chamber for each O_2 flow rate was 0.1 sccm ($1.3 x 10^{-5}$ torr), 0.3 sccm ($9.2 x 10^{-4}$ torr) and 1.6 sccm ($4.8 x 10^{-3}$ torr). The deposition time was 35 mins which corresponds to a thickness of ~ 17 nm as measured by ellipsometry. During the deposition the substrate was not heated.

Synthesis of TaO_x by RF sputtering

TaO_x was deposited onto p-Si using a reactive sputtering AJA international ATC orion 5 tool equipped with a load lock chamber. A pure Ta sputtering target was used with a RF power of 150 W. The deposition pressure was 3mTorr under an atmosphere of ($Ar+O_2$). Ar to O_2 ratio was varied from 90:10, 96:4, 97:3 and 99:1. Different times of deposition was evaluated (20s to 3 min) yielding thickness of TaO_x (20 to 180 nm). The thickness was measured with a quartz crystal monitor during

deposition. Only 97:3 and 99:1 yielded decent photocurrent densities and hence was pursued in depth in this work. Prior to deposition, the Ta target was presputtered for a period of 30 min to remove any oxide layer on the Ta target.

Sputtering of Cu and Au Co-catalyst

Sputtering of Cu and Au co-catalyst was performed in the same sputtering as TaO_x. Pure Cu and Au targets were used with a RF power of 100 and 150 W respectively. The deposition pressure was 3 mTorr under an Ar atmosphere. The thickness of Cu was varied from 5-20 nm and Au thickness was 5 nm (all thicknesses were measured by a quartz crystal monitor).

SEM and EDX characterization

The SEM and EDX characterization were performed using a zeiss gemini ultra-55 analytical field emission scanning electron microscopy that is coupled a Bruker X-rau energy dispersive spectrometer.

XRD characterization

The crystallinity of the thin films and the photocathode was analyzed by X-ray diffraction with a Rigaku Smartlab diffractometer using Cu Kα radiation.

XPS characterization

Chemical composition of TaO_x films were obtained by XPS on a Kratos Axis Ultra DLD system at a take-off angle of 0° relative to the surface normal. An Al Kα source (hν = 1,486.6 eV) was used with a pass energy of 20 eV for the narrow scan of core levels and valence band spectra with a step size of 0.05 eV and 0.025 eV, respectively. The spectral fitting was conducted using CasaXPS analysis software.

Photoelectrochemical testing of CO_2R photocathodes

All photoelectrochemical measurements were performed using a Biologic SP-300 potentiostat under simulated AM 1.5 G illumination, calibrated using a silicon diode. Details about the polyetheretherketone (PEEK) cell employed for CO2R can be found in our prior work.[1] The PEEK cell was cleaned in nitric acid and DI water before every measurement. The working electrode (Si-TaO_x/Cu or Au) was connected to a Cu back contact with a In-Ga eutectic. The counter electrode

used was a Pt wire and a leak free Ag/AgCl reference electrode was used. After the assembly of the cell, the electrolyte (0.05M K_2CO_3) was bubbled with CO_2 at a flow rate of 5 sccm and the volume of the electrolyte employed in both the cathode and anode chamber was 2 ml. Potentiostatic Electrochemical Impedance Spectroscopy (PEIS) in the dark was performed to measure the resistance of the solution. PEIS was performed from 1 MHz to 100 Hz to obtain the correct frequency in determining Rs (10 kHz). The VSP-300 potentiostat's IR compensation function only compensates 85% of Rs, thus the remaining 15% of Rs was corrected manually. Final voltage calculation after 100% IR compensation is as below:

$V100\%IR_s$ (RHE) = V85% IR (RHE) + 15% average R_s (Ohms) * average I (A).

Gas product quantification by gas chromatography (GC)

A SRI 8610C Gas chromatograph is used to detect and quantify the gas products. The four gas phase CO2R products (CO,CH_4,C_2H_4 and C_2H_6) and H_2 were detected and quantified using the calibration curves by injected known concentrations of gaseous products (Figure S1). Briefly in GC The CO2 was continuously flowing through the PEC cell; a portion of the exiting gas is directed into the sampling loops of the gas chromatograph. Two channels were used. Channel 1 comprises a 6' Heysep-D and a 6' Molsieve 13x column, a 1 ml sampling loop, Ar carrier gas and H2 for flame ignition. This channel is S12 equipped with a flame ionization (FID) detector and a methanizer for CO to CH4 conversion. Channel 1 has the ability to detect the CO, CH_4, C_2H_4 and C_2H_6. Channel 2 has a 6' Heysep-D column, a 2 ml sampling loop, and N_2 carrier gas. This is equipped with a TCD detector for H_2 detection. Calibration curves are shown in Figure S1.

The Faradaic efficiency of the CO_2 reduction gaseous products is estimated using the equation below

$$FE(\%) = \frac{F \times n \times x \times F_{CO2}}{I}$$

where F is the Faraday constant (96485 C mol^{-1}), n is the number of the electrons required for a particular CO_2 reduction product, x is the mole fraction of the gaseous product obtained from the GC, F_{CO2} is the molar flow rate of CO_2 through the cell, and I is the average current during the run. The number of electrons required are 2, 8, and 12 for CO, CH_4 and C_2H_4.

Liquid products quantification by NMR

The quantification of liquid products using 1D ^{1}H NMR(Bruker 500 MHz) using 50 mM phenol and 10 mM dimethyl sulfoxide (DMSO) as the internal standards for quantification. The water peak was suppressed by a presaturation sequence. 400 µL of electrolyte after CO_2 photoelectrolysis was added to 50 µL of D_2O and 50 µL of internal standard solution. To determine the concentration of each CO_2R product, the area of their corresponding peak should be compared with the area of the standards. For all peaks on the left side of the water peak (> 4.7 ppm), the phenol is the calibration standard. For all peaks on the right side of the water peak (< 4.7 ppm), DMSO is the calibration standard. The product were identified using the work of marc Robert.[3] The concentration of each product $C_{product\ tube}$ in the tube can be computed using the following equation.

$$C_{product} = C_{standard\ tube} \times \frac{\frac{A_{Product}}{H_{product}}}{\frac{A_{standard}}{H_{standard}}}$$

A corresponds to the area of the peak and **H** corresponds to the number of protons corresponding to this peak. Finally, the faradaic efficiency of the liquid product can be computed using the following equation.

$$FE = \frac{C_{product} \times V_e \times n \times F}{I \times t}$$

V_E corresponds to the volume of the electrolyte; n is the number of the electrons required for a particular CO_2R product, t corresponds to the duration of the electrochemical test [s] and $C_{product}$ corresponds to the concentration of product in the electrolyte

Techno-economic analysis

Techno-economic analysis was performed deploying a recently proposed protocol for assessment of emerging electrolysis technologies (M. H. Barecka et al., 2021b). Following data was introduced to the calculation tool attached to the protocol; this dataset is derived from our experiments and the goals defined for the technology scale-up:

- Current density: 0.01 A/cm^2
- Voltage: 1.2 V

- CO$_2$ conversion: 75%

- Faradaic Efficiences : 20% ethylene, 2% carbon monoxide, 8% methane, 4% hydrogen,

- Electrode size : 50,000 m^2

- Market price of electrolysis product stream: 0.1 \$/kg (as reported for syngas streams) (M. H. Barecka et al., 2021a)

We subsequently assessed the flow of the products obtained from such system and calculated the value as a function of the imposed CO$_2$ tax credit, calculated using the Equation 1. The CO$_2$ credit is assumed to be imposed proportionally to the stochiometric amount of CO$_2$ emissions resulting from combustion of produced amount of ethylene, carbon monoxide and methane. Using our method, these compounds are obtained from biogenic CO$_2$ thus the production method allows to avoid the emissions which would be otherwise associated petroleum-based methods.

$$Electrolysis\ stream\ value \tag{1}$$
$$= market\ price + \ (88/28 \cdot ethylene\ fraction + 44/16$$
$$\cdot methane\ fraction + 44/28 \cdot carbon\ monoxide\ fraction)$$

To assess the investment cost into photoelectrocatalytic system, we consider all components of a large reactor that include cathode material, selemion membrane, anode material based on platinum group metal, the balance of the plant including e.g. necessary power connection and installation costs (see Supplementary Table 1 with data for Cu electrode and Supplementary Table 2 for Au electrode).

To evaluate the return on investment, the total investment into the photoelectrocatalytic system was divided by value generated yearly, which is a function of the CO$_2$ credit and electricity price.

The results of the sensitivity analysis for Au-based systems are given in Supplementary Figure S16.
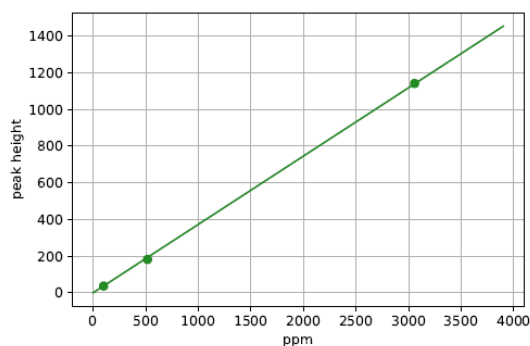
Supplemental figures
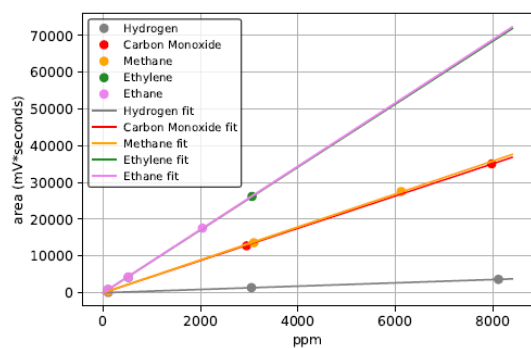
(a) All the gas measured.
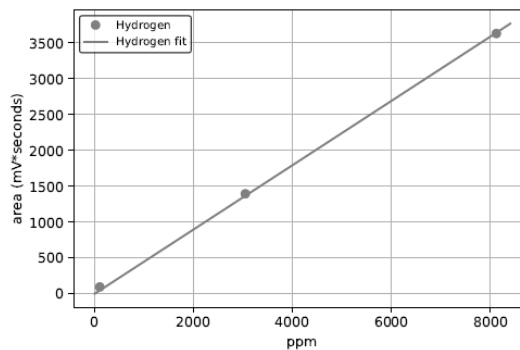
(b) Hydrogen calibration curve.

(c) Ethylene calibration curve.

Figure S1. (a) Calibration curves for all the gas products measured (CO, CH_4, C_2H_4 and C_2H_6 and H_2) (b) H_2 calibration and (c) magnified view of the C_2H_4 calibration data from (a).
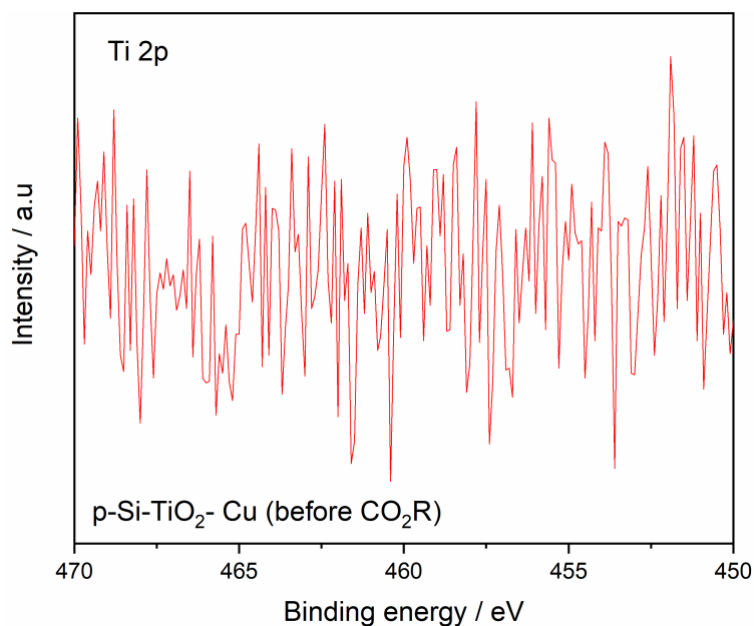
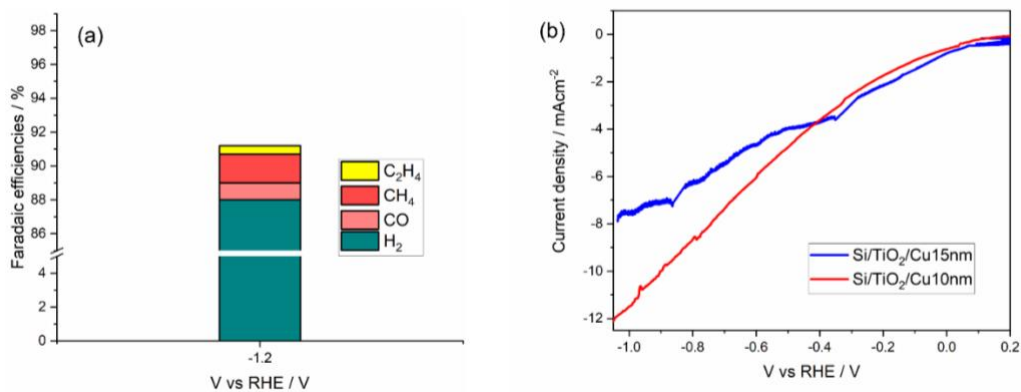**Figure S2**. XPS Ti 2p core level spectra of p-Si/TiO₂/Cu(10nm) before CO₂R electrolysis.

Figure S3. (a) Faradaic efficiencies of CO₂R products for Si/TiO₂/Cu15 nm under 1 sun illumination in 0.1M KHCO₃. **(b)** Current density (J) vs Voltage (V) plots for Si/TiO₂/Cu10 nm and Si/TiO₂/Cu15 nm under 1 sun illumination in 0.1M KHCO₃
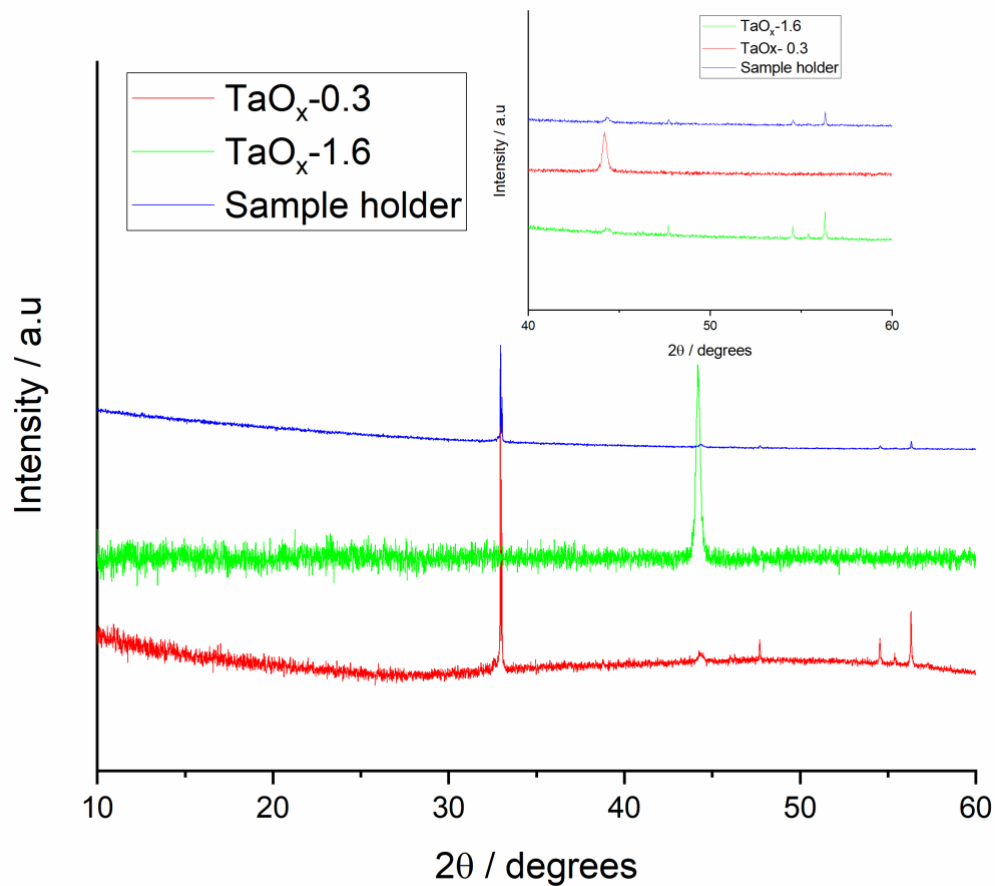
Figure S4. XRD patterns for PLD-grown TaO_x-0.3 and TaO_x-1.6 grown on glass substrates showing the amorphous nature of the PLD-grown films. The XRD peaks observed were from the sample holder of the XRD and peaks corresponding to tantalum oxide phases were not observed.
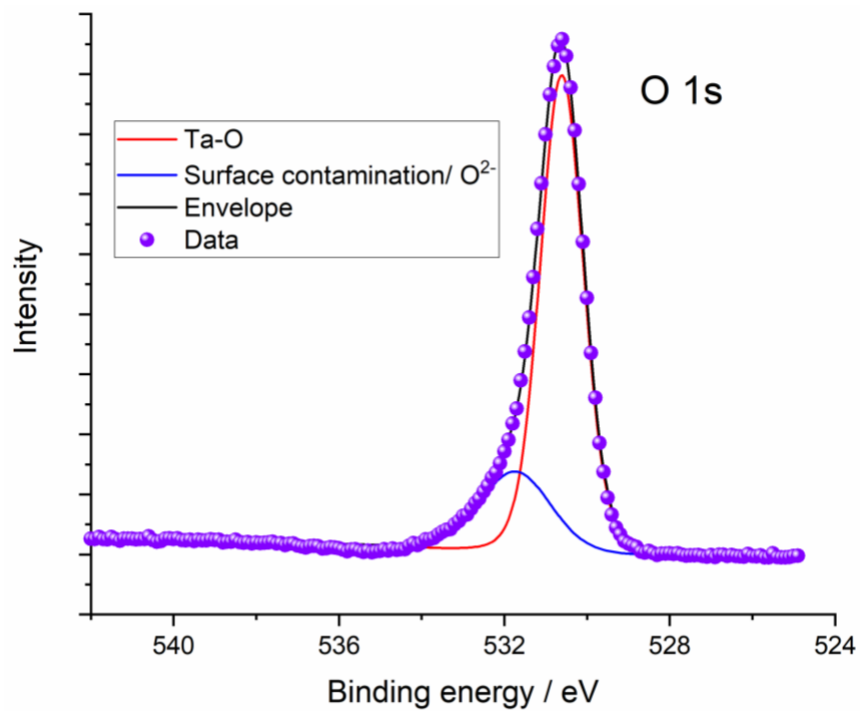
Figure S5. Core level O 1s spectrum of TaO$_x$-0.3 PLD grown film.
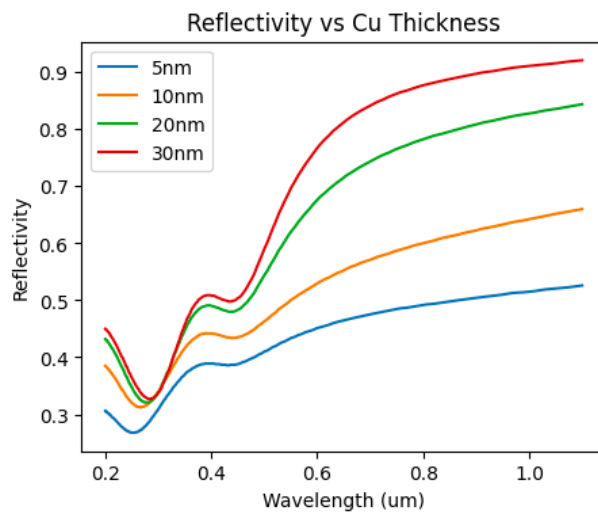
Figure S6. Finite-difference time-domain (FDTD) simulations using MEEP to estimate the reflectivity of Si/TaO$_x$/Cu stacks with varying Cu thickness.
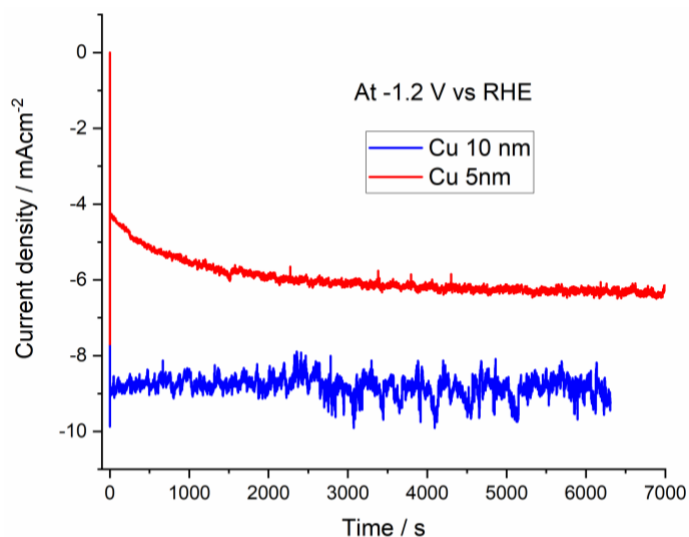
Figure S7. Current vs time plots for p-Si/TaO$_x$-0.3/Cu-5nm and p-Si/TaO$_x$-0.3/Cu-10nm at -1.2 V vs RHE under 1 sun illumination in CO$_2$ saturated 0.1 M KHCO$_3$ showing the lower photocurrent density observed with Cu-5nm.
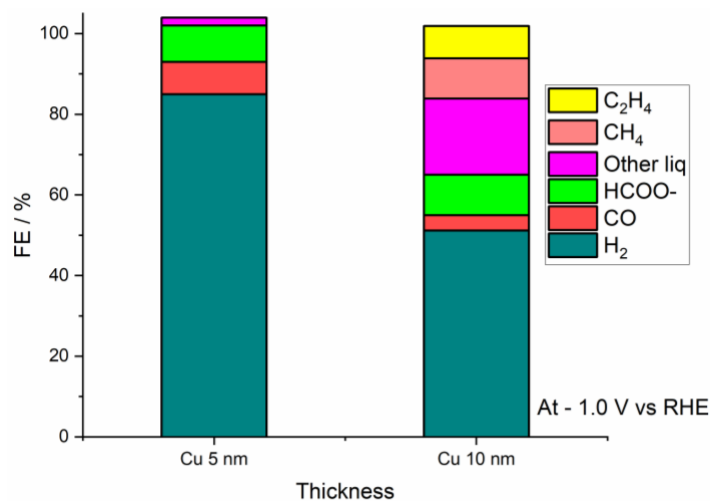
Figure S8. Comparison of the product distribution different Cu thickness at -1.0 V vs RHE for p-Si/TaO$_x$/Cu under 1 sun illumination in CO$_2$ saturated 0.1 M KHCO$_3$. More CO$_2$R products were observed for Cu catalyst thickness of 10 nm.
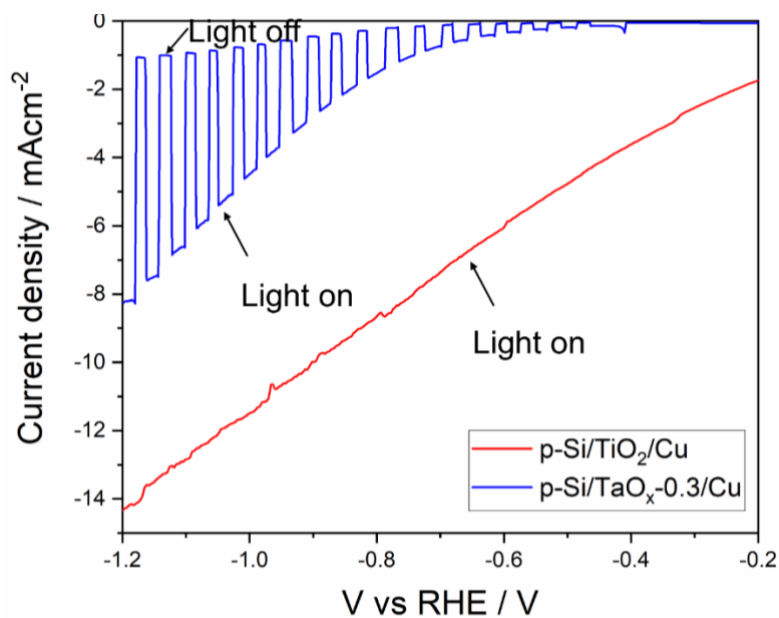
Figure S9. Comparison of current density vs Voltage plots for p-Si/TiO$_2$/Cu and p-Si/TaO$_x$-0.3/Cu showing earlier onset of photocurrent density for p-Si/TiO$_2$/Cu. Cu thickness of 10 nm was employed for both devices.
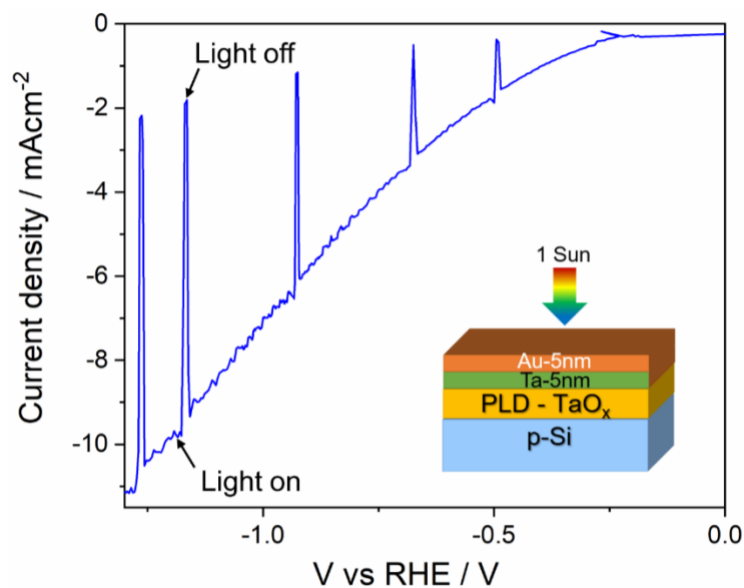
Figure S10. Current density vs Voltage plots of p-Si/TaO$_x$-0.3/Ta/Au photocathode under 1 sun illumination in 0.1 M KHCO$_3$.
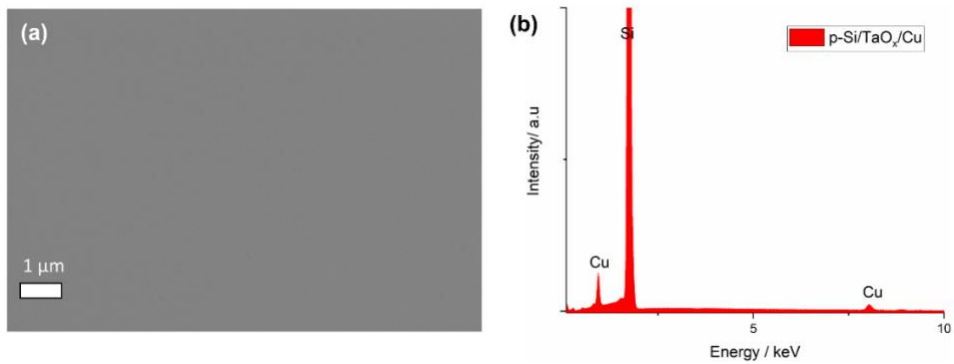
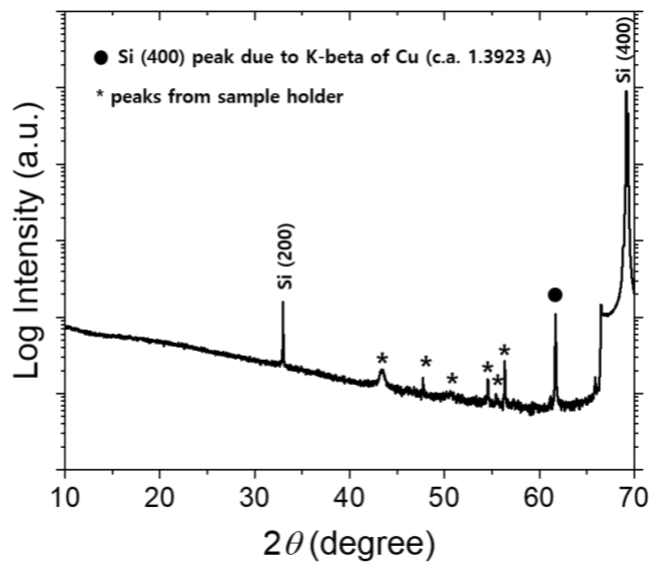**Figure S11. (a)** SEM top view and **(b)** EDX spectrum of p-Si/TaO$_x$/Cu photocathode.

Figure S12. XRD pattern of p-Si/TaO$_x$ (sputtered)/Cu(10nm) photocathode.
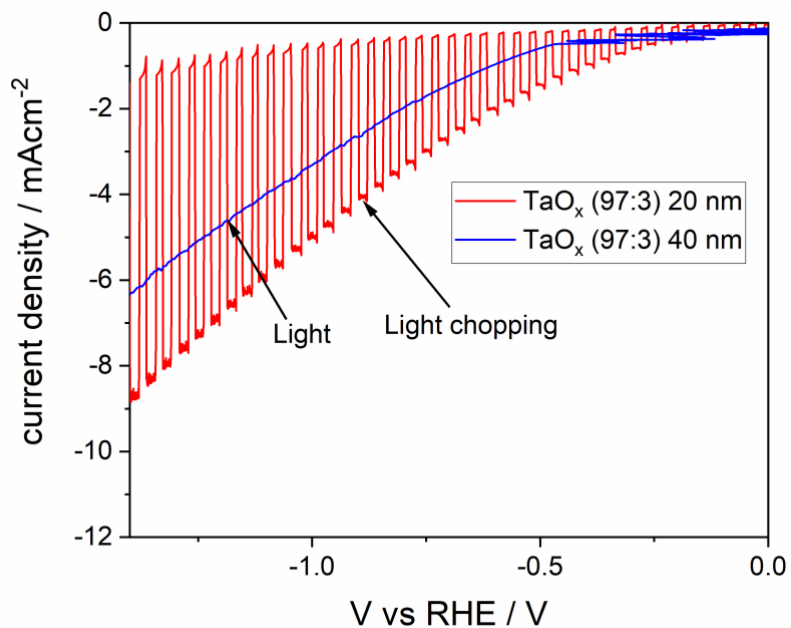
Figure S13. Comparison of Current density vs Voltage plots of p-Si/TaO$_x$(97:3)/Cu photocathode for 2 different thickness of the TaO$_x$ (20 and 40 nm) under 1 sun illumination in 0.1 M KHCO$_3$ showing a later photocurrent onset and poorer fill factor for 40 nm TaO$_x$ thickness.
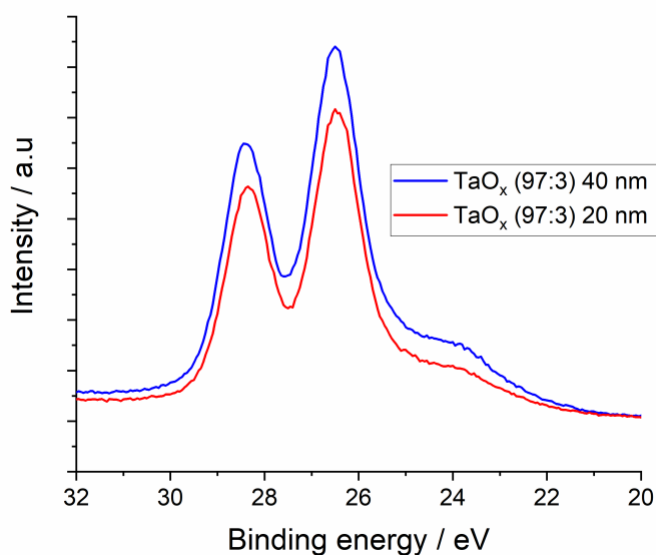

Figure S14. Ta 4f core level spectra of 20 and 40 nm thick TaO$_x$ with an Ar:O$_2$ ratio of 97:3.
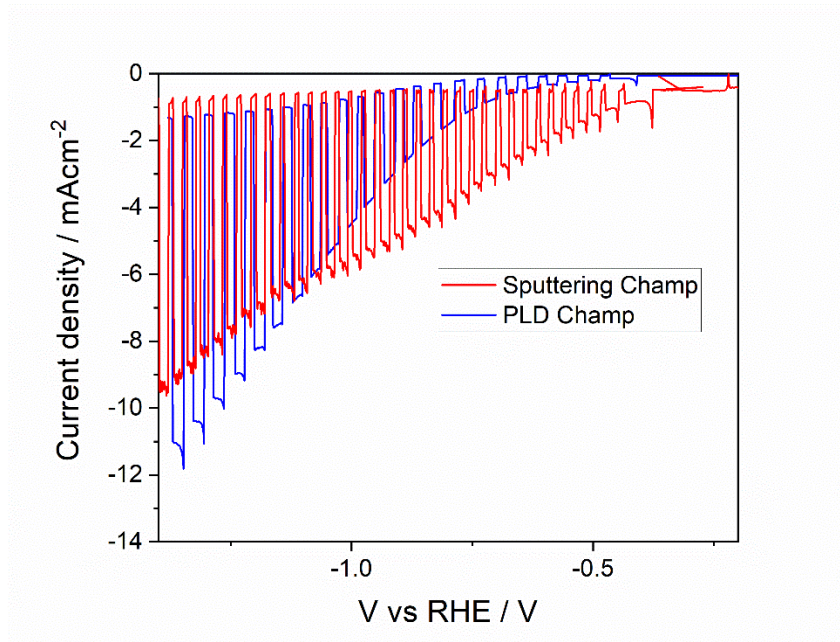
Figure S15. Comparison of the Current density vs Voltage plots for the champion (Champ) device prepared by PLD and Sputtering under 1 sun illumination in 0.1 M KHCO$_3$.
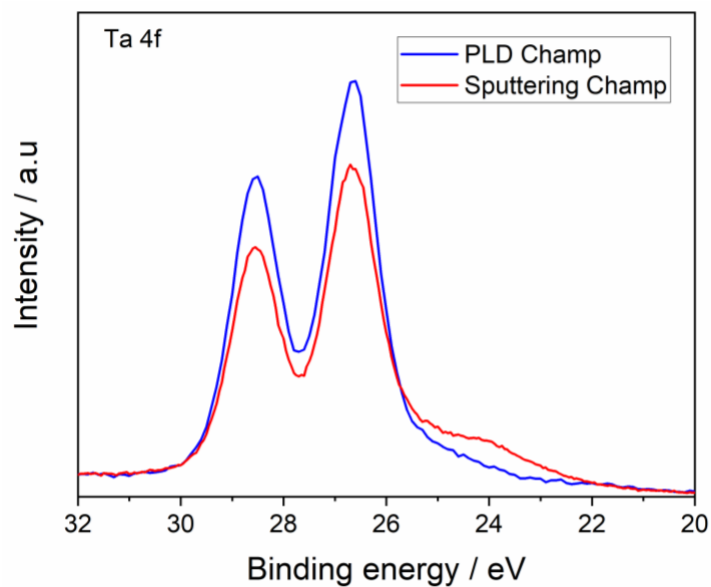

Figure S16. Comparison of Ta 4f core spectra of TaOx-0.3 prepared by PLD and TaO$_x$ (97:3) prepared by RF sputtering which yielded the best PEC performance (champion device).
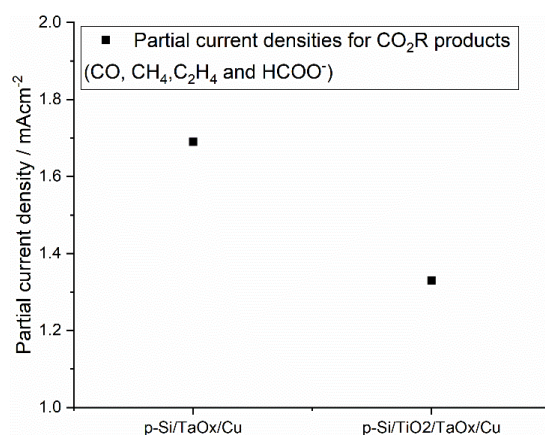
Figure S17. Partial current densities for CO_2R products (CO, CH_4, C_2H_4 and $HCOO^-$) for p-Si/TaO$_x$/Cu (RF sputtered TaO$_x$) and dual ETL photocathode (p-Si/TiO$_2$/TaO$_x$/Cu).
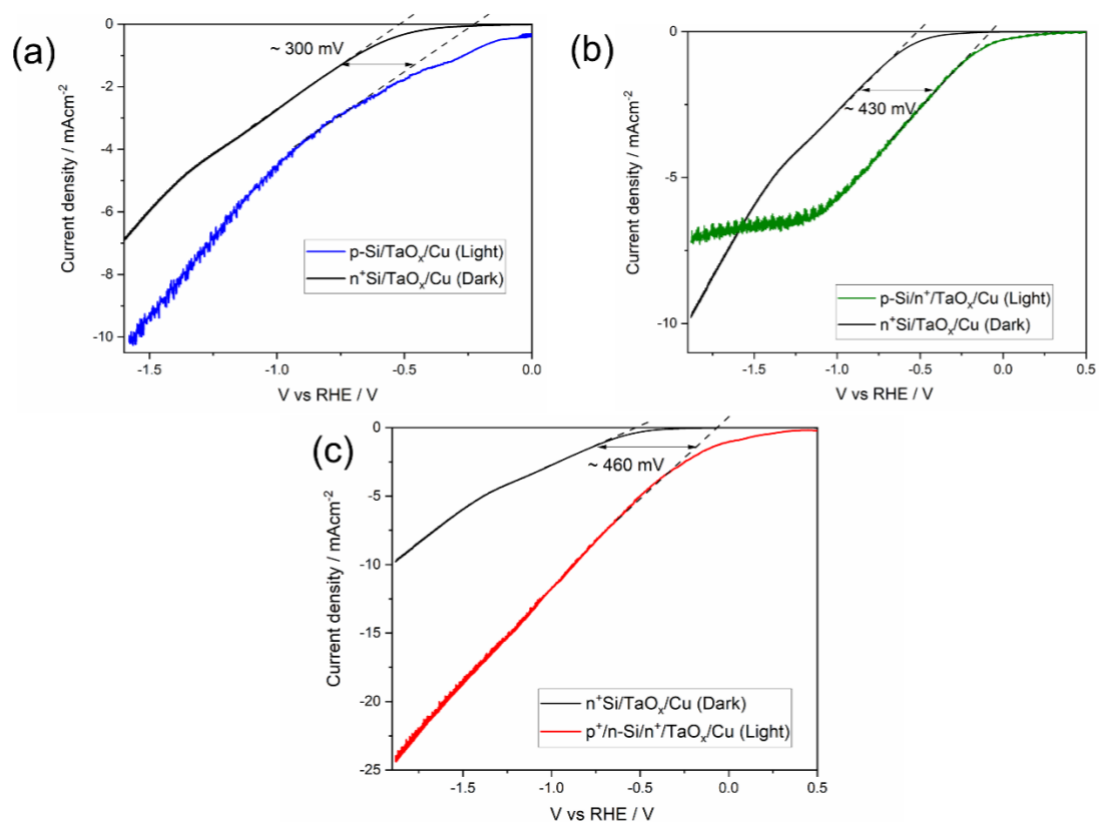

Figure S18. Estimation of photovoltage for (a) p-Si/TaO$_x$/Cu (b) p-Si/n$^+$/TaO$_x$/Cu (c) p$^+$/n-Si/n$^+$/TaO$_x$/Cu photocathode by comparing with the dark cathode of n$^+$Si/TaO$_x$/Cu.
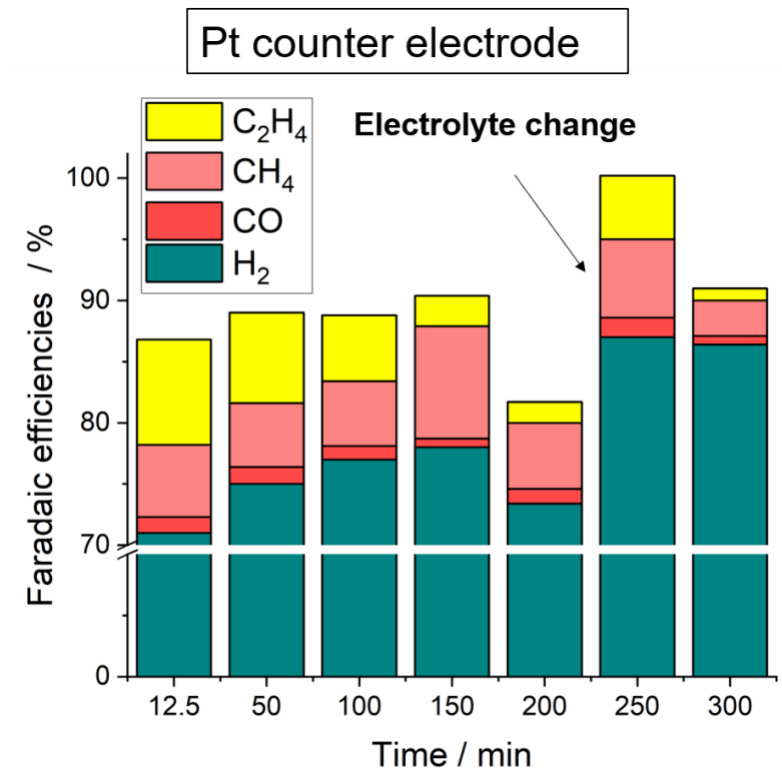
Figure S19. Gaseous CO_2R product distribution as a function of time for $Si/TaO_x(97:3)/Cu10nm$ photocathode under 1 sun illumination in 0.1 M $KHCO_3$ at -1.2 V vs RHE with a Pt counter electrode. Electrolyte was changed after 225 mins and then C_2H_4 production increased and quickly reduced. There was also observable Pt migration from the counter electrode to the photocathode which could explain the increased HER and reduced CO_2R product evolution This has been observed in prior reports by Ren et al[4] and Gurudayal et al[1] where metal crossover from the counter electrode has resulted in increased HER activity. Given the 2 set of results from our experiments, first the reduced hydrophobicity of the surface and second the Pt migration from the counter electrode, the most likely cause for increased HER activity is the Pt migration onto the photocathode. Given the thin Cu catalyst thickness we employ ~ 10 nm, even a nanometer scale Pt migration would have a drastic effect in reducing the CO_2R catalytic activity and favoring HER.
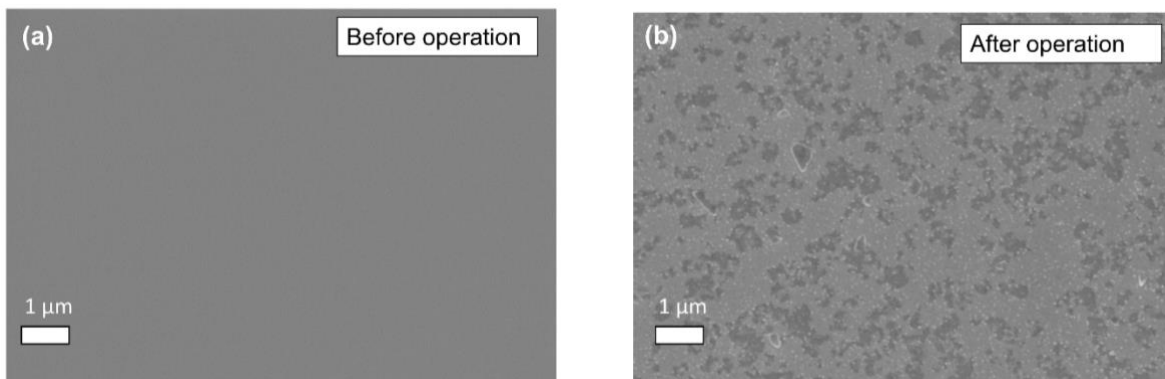
Figure S20. SEM top view image of p-Si/TaO$_x$(97:3)/Cu(10nm) photocathode (a) before CO$_2$R electrolysis and (b) after CO$_2$R electrolysis.
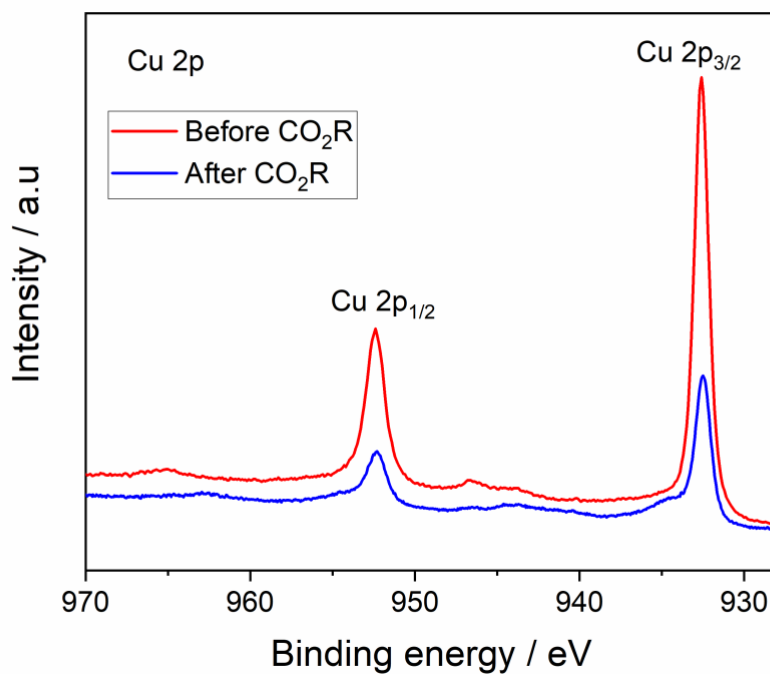

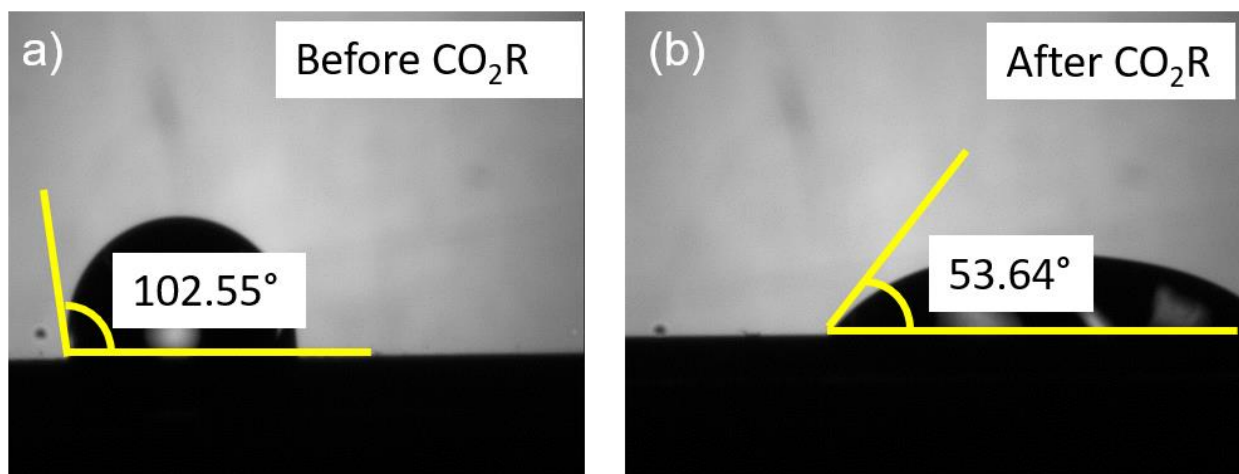**Figure S21.** Cu 2p core level spectra of Si/TaO$_x$(97:3)/Cu before and after CO$_2$R operation for 300mins.

Figure S22. Contact angle measurements of p-Si/TaO$_x$/Cu photocathode with a Pt counter electrode during CO$_2$R measurements for (a) before CO$_2$R and (b) after CO$_2$R operation for 300 mins.
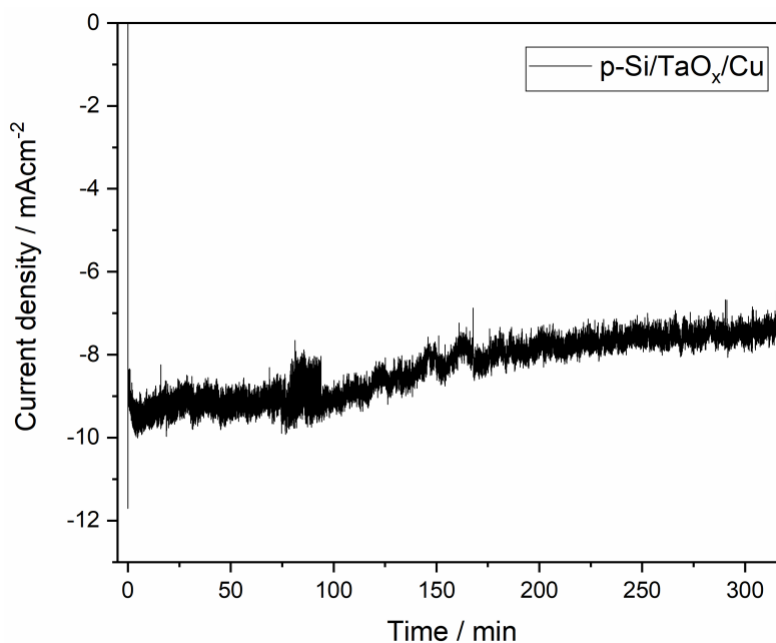

Figure S23. Current density vs Time plots for p-Si/TaO$_x$(97:3)/Cu10nm photocathode under 1 sun illumination in 0.1M KHCO$_3$ at -1.2 V vs RHE with a graphite counter electrode.
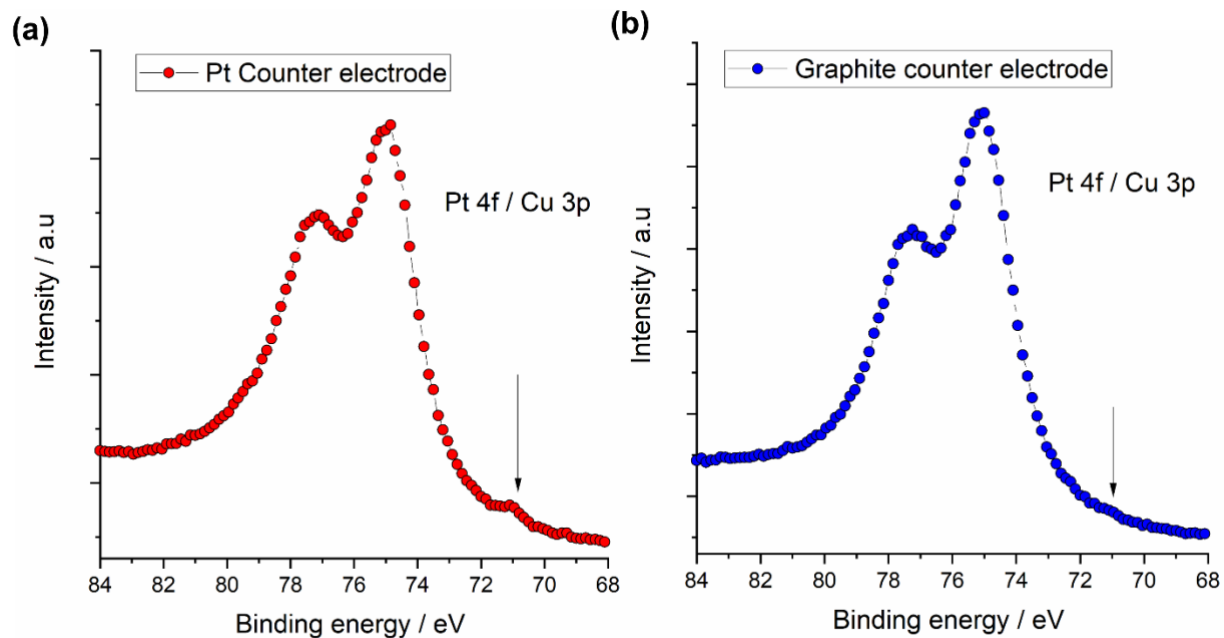
Figure S24. (a) Cu3p/Pt 4f core level spectra of Si/TaO$_x$ (97:3)/Cu after CO$_2$R showing the migration of Pt from the Pt counter electrode to the photocathode (Pt 4f 71 eV). (b) Cu3p/Pt 4f core level spectra of Si/TaO$_x$ (97:3)/Cu after CO$_2$R showing no Pt from the graphite counter electrode to the photocathode (Pt 4f - 71 eV).[5]

Supplementary tables

Supplementary Table 1.

Input data for the assessment of the investment cost for manufacturing of **Cu-based photoelectrodes**. The cost of catalyst deposition is assessment based on pilot-plant/semi-industrial coefficients for the energy use in PVD deposition process, and the most recent price indicators for silicon, membranes, and metal cost.

Membrane cost $/m^2	500 [6]
Platinum group metal and ionomer cost $/m^2	38 [6]
Energy cost for sputtering $/m^2 (industrial benchmark: 7.53E-05 kWh/cm^2)	0.015 [7]
Argon cost $/m^2 (industrial benchmark: 1.21E-7 m^3/cm^2)	3.63E-05 [7]
Oxygen cost $/m^2 (industrial benchmark: 9.88E-10 m^3/cm^2)	8.47E-07 [7]
Silicon wafer cost $/m^2	1116 [8]
Cu cost $/m^2 for 10 nm layer	0.001 [9]
Ta$_2$O$_5$ cost $/m2 17 nm layer	0.022 [10]
Total cost $/m^2	1654.143
Balance of the plant (BoP)	1.3
Installation factor	1.2
Total cost for the designed electrolyzer ($M) 50,000 m^2	129.0

Supplementary references

1   Gurudayal, J. W. Beeman, J. Bullock, H. Wang, J. Eichhorn, C. Towle, A. Javey, F. M. Toma, N. Mathews and J. W. Ager, *Energy Environ. Sci.*, 2019, **12**, 1068–1077.

2   Y. Li, S. Sanna, K. Norrman, D. V. Christensen, C. S. Pedersen, J. M. G. Lastra, M. L. Traulsen, V. Esposito and N. Pryds, *Appl. Surf. Sci.*, 2019, **470**, 1071–1074.

3   T. Chatterjee, E. Boutin and M. Robert, *Dalt. Trans.*, 2020, **49**, 4257–4265.

4   D. Ren, N. W. X. Loo, L. Gong and B. S. Yeo, *ACS Sustain. Chem. Eng.*, 2017, **5**, 9191–9199.

5   I. Roh, S. Yu, C.-K. Lin, S. Louisia, S. Cestellos-Blanco and P. Yang, *J. Am. Chem. Soc.*, 2022, **144**, 8002–8006.

6   A. Mayyas, M. Ruth, B. Pivovar, G. Bender and K. Wipke, Manufacturing Cost Analysis for Proton Exchange Membrane Water Electrolyzers, https://www.nrel.gov/docs/fy10osti/72740.pdf.

7   M. Barecka, A. Zieminska and I. Zbicinski, *INREP Proj. Rev. http//www.inrep.eu/files/TCO%202017/INREP_TCO2017_Presentation_TUL_170921.pdf*.

8   M. Tyson, Silicon Wafer Prices Expected to Increase by up to 25% by 2025 | Tom's Hardware, https://www.tomshardware.com/news/silicon-wafer-prices-expected-to-rise-by-up-to-25-by-2025.

9   MacroTrends, Copper Prices - 45 Year Historical Chart | MacroTrends, https://www.macrotrends.net/1476/copper-prices-historical-chart-data.

10 Statista, Tantalum price 2021 | Statista, https://www.statista.com/statistics/1009173/tantalum-price/.